nature nanotechnology

REVIEW ARTICLE

PUBLISHED ONLINE: 5 FEBRUARY 2013 | DOI: 10.1038/NNANO.2012.265

Multi-electrode array technologies for neuroscience and cardiology

Micha E. Spira* and Aviad Hai

At present, the prime methodology for studying neuronal circuit-connectivity, physiology and pathology under *in vitro* or *in vivo* conditions is by using substrate-integrated microelectrode arrays. Although this methodology permits simultaneous, cell-non-invasive, long-term recordings of extracellular field potentials generated by action potentials, it is 'blind' to subthreshold synaptic potentials generated by single cells. On the other hand, intracellular recordings of the full electrophysiological repertoire (subthreshold synaptic potentials, membrane oscillations and action potentials) are, at present, obtained only by sharp or patch microelectrodes. These, however, are limited to single cells at a time and for short durations. Recently a number of laboratories began to merge the advantages of extracellular microelectrode arrays and intracellular microelectrodes. This Review describes the novel approaches, identifying their strengths and limitations from the point of view of the end users — with the intention to help steer the bioengineering efforts towards the needs of brain-circuit research.

A central goal of contemporary neuroscience is to understand the relationships between the functional connectivity-map of neuronal circuits and their physiological or pathological functions. At present, this goal seems impossible to achieve as available electrophysiological technologies only allow for extracellular recordings of large populations of neurons and are not suitable for providing simultaneous intracellular recordings of neural activity from hundreds of individual neurons. Furthermore, because of their mechanical instability, intracellular glass electrodes cannot be used to monitor long-term electrophysiological correlates of plasticity and learning. An ideal multiunit readout system should provide information that covers the entire repertoire of electrophysiological parameters from the individually recorded neurons. These include: action potentials (APs), subthreshold excitatory- and inhibitory-postsynaptic potentials (EPSPs and IPSPs, respectively), and subthreshold membrane oscillations. Moreover, it should be possible to modulate the activity of individual neurons within the network by current application.

The available methodologies for the recording of neural activity include: (a) intracellular recordings and stimulation by sharp or patch electrodes, (b) extracellular recordings and stimulation by substrate-integrated microelectrode arrays (MEAs), (c) optical imaging and stimulation technologies of extrinsic fluorescent indicators or genetically encoded molecular probes, and (d) other methods such as functional magnetic resonance imaging, electroencephalography, electrocorticography and magnetoencephalography, designed to record activity from very-large-scale neural populations, which are not suitable for single-neuron resolution.

The invention of intracellular recording and stimulation technologies were hallmark developments that enabled the biophysical 'language' by which individual neurons transmit electrical information, communicate and 'compute' subthreshold synaptic information to be deciphered[1–4]. The power of intracellular recording systems is that they exhibit very good electrical coupling with the cell and provide accurate readout of the entire dynamic range of voltages generated by cells without distorting the readout over time. Yet, the use of sharp or patch microelectrodes is limited to individual neurons as steering of the electrode tips into target cells requires the use of bulky micromanipulators and the duration of intracellular recording sessions is limited by mechanical and biophysical instabilities.

In contrast, whereas the use of cell-non-invasive extracellular MEAs for *in vitro* recordings and polytrodes for *in vivo* recordings largely attenuate and temporally filter the electrical signals, it enables the simultaneous recording and stimulation of large populations of excitable cells for days and months without inflicting mechanical damage to the neuron's plasma membrane[5–10]. Extracellular field potential recordings (ambiguously referred to as local field potentials (LFPs) or field potentials (FPs)) reflect the spike activity of individual neurons or the superposition of fast APs, synaptic potentials and slow glial potentials in both time and space. As the physical processes that underlie the generation of FPs are understood it is theoretically possible to reconstruct their sources. Even though a great deal of information can be gained by using polytrodes, the information harboured in spike-pattern fingerprints is limited[11]. For example, extensive spike sorting cannot provide information as to whether the firing of an individual neuron is triggered by endogenous mechanisms, a barrage of incoming excitatory inputs or the cessation of inhibition (Box 1). What terminates the firing of a given neuron? Is it a barrage of inhibitory synaptic inputs, cessation of excitatory inputs or hyperpolarization of the membrane potential by endogenous mechanisms? Neurons that do not fire APs during a recording session are not 'visible' to extracellular electrodes (referred to as 'dark neurons'; Box 1). In some brain areas, 90% of the neurons are not spiking or are firing occasionally at very low rates of <0.16 spikes per second (for review see ref. 12). Intracellular recordings of synaptic potentials from such neurons would disclose a great deal of information as to the role of this 'silent majority' in information processing and the importance of individual neurons to the circuit behaviour. A great deal of neuroplasticity is associated with changes in the amplitude of synaptic potentials[13]. Unless these changes reach firing threshold, extracellular recording systems are 'blind' to these critical events. It is conceivable that significant signalling between neurons is mediated by subthreshold potentials (chemical or electrical synapses) and is thus undetectable by conventional extracellular electrodes.

The Alexander Silberman Life Sciences Institute, and the Harvey M. Kruger Family Center for Nanoscience, The Hebrew University of Jerusalem, Jerusalem 91904, Israel. *e-mail: spira@cc.huji.ac.il

Box 1 | Illustration of some of the limitations of extracellular recordings with respect to intracellular recordings.

Endogenous membrane properties as well as excitatory and inhibitory synaptic inputs regulate the firing patterns of individual neurons. This is depicted in the schematic of a neuron (blue) that receives an excitatory and an inhibitory synaptic input in **a**. Subthreshold and supra-threshold electrophysiological activity of the neuron is recorded by an intracellular (upper orange electrode) and an extracellular (lower orange electrode) electrode. The amplifiers are depicted in yellow. The intracellular recordings are shown in the left panels of **b**–**e**, and the corresponding extracellular recordings are shown in the right panels (green background). In **b**, a neuron endogenously generates a train of APs (of approximately Δ100 mV) by depolarization of the membrane potential from the resting value of approximately −80 mV (bottom dashed line) reaching a threshold level to fire APs (middle dashed line) at about −50 mV, and then the membrane potential endogenously repolarizes. The extracellular electrode picks up the FPs generated by the APs (marked by vertical lines and green background). Note that the recorded FP amplitudes range between 0.01 and 1 mV, and are not drawn to scale. The attenuation factor (1/100 to 1/1000) is so large that subthreshold potentials generated by individual neurons cannot be recorded. Thus, the extracellular electrode is practically 'blind' to the subthreshold events (grey background, below the red dashed line). In **c** and **d** the very same pattern of APs firing is generated by excitatory (**c**) and inhibitory (**d**) synaptic inputs. Whereas in **c** summation of excitatory synaptic potentials depolarizes the neuron to reach the firing level, and the neuron stops firing when the barrage of the excitatory inputs stops (leading to membrane repolarization), in **d** the train of APs is generated by dis-inhibition (the cessation of the barrage of inhibitory synaptic inputs). The significant differences in these mechanisms (**b**–**d**) cannot be detected by the extracellular electrode. Furthermore, unless an individual neuron is firing APs, synaptic inputs are not 'visible' to the extracellular electrodes at all (**e**). In this example, the extracellular electrode does not detect the presence of a neuron that receives a barrage of excitatory and inhibitory synaptic inputs. These inputs may be of significant importance to the functioning of the neuronal circuit.

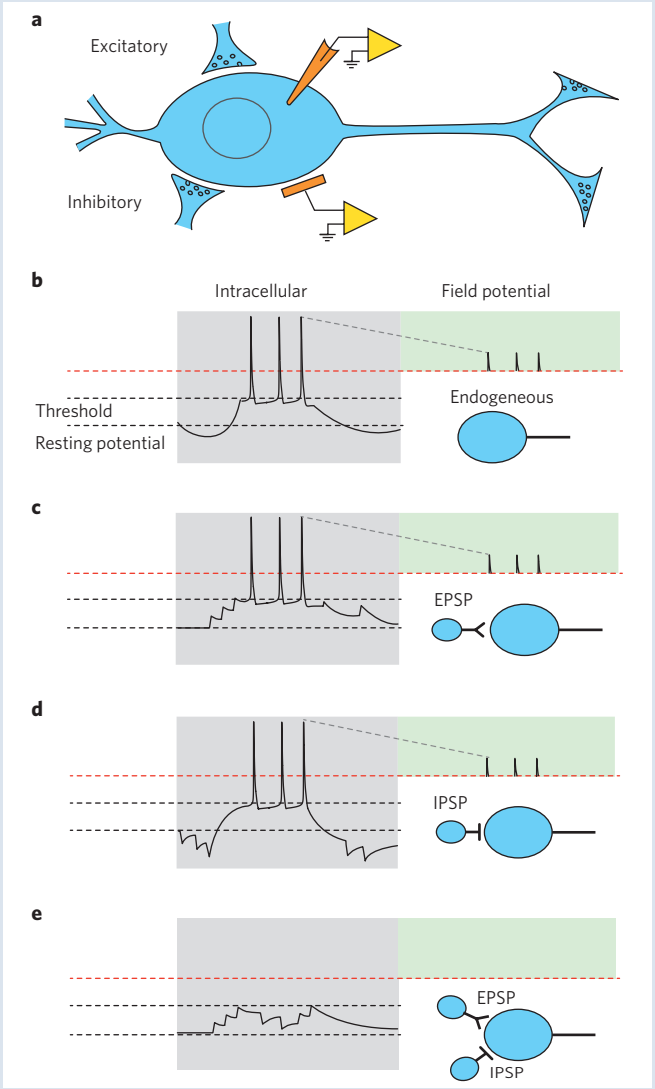

Since the development of the first MEA[14–17], technological efforts improved the quality of information gained by extracellular recordings mainly by increasing the density and the number of the electrodes that can be constructed and addressed over a single MEA. *In vitro* MEAs may contain over 10,000 electrodes[5,7,8,18,19]. *In vivo* polytrodes may have over a hundred[9,20]. Nevertheless, the recording and stimulation qualities of these platforms (reflected by the electrical coupling coefficient between single neurons and the device, and the signal-to-noise ratio) remained poor. Typically the amplitudes of FPs range between 10 μV to 1 mV and a great deal of computational power is required to extract data and sort out the recorded signals[21,22].

In parallel to the development of the extracellular MEA, efforts to develop optical imaging approaches began. These included imaging of membrane potentials by the use of voltage-sensitive dyes[23–27], imaging of neuronal activity by monitoring the changes in the free intracellular calcium concentration[28–30] and the monitoring of intrinsic signals[31]. This was followed by very powerful methods to optically excite or inhibit individual neurons or neuronal ensembles[32,33]. The powerful optical imaging methods suffer from a number of limitations that at present prevent them from replacing electrophysiological approaches for studying neuronal circuits (for discussion see ref. 34).

Using nano- and micro-technologies, a number of laboratories began to merge the advantages of substrate-integrated extracellular MEA technologies with the critical advantages of intracellular electrodes. Namely, the construction of nano- or microdevices that enable simultaneous, long-term, multisite, intracellular recording and stimulation from many neurons under *in vitro* conditions. Further development and implementations of these technologies are expected to revolutionize basic and applied neuroscience.

In this Review we describe recent developments, expected benefits from their use and the foreseen limitations of the different approaches. We review these developments from the end-user point of view, rather than from the technological point of view. By considering the needs of contemporary 'circuit neuroscience' on the one hand and the recent technological developments in MEA fabrication on the other, we hope to shift the focus of upcoming technical developments from the habitual engineering optimizations to the pressing needs of neuroscience.

To objectively evaluate the different approaches, we examine the principal achievements in relation to a list of biophysical parameters that are needed to decipher the functional connectivity map of a neuronal network. An ideal imaginary device would allow the user to: (a) simultaneously record and stimulate hundreds of individual

neurons intracellularly, (b) maintain a stable contact with the neurons for recording and stimulation for days and months, (c) monitor the transmembrane potential in the relevant cell-physiological range of −80 to +30 mV, (d) detect subthreshold potentials such as excitatory and inhibitory synaptic potentials with amplitudes in the range of ±0.5–10 mV with a rise time of <1 ms and a slow decay time of 100–1,000 ms, and to record membrane oscillations in the range of ±5 mV at frequencies of 1–50 Hz, (e) record APs with amplitudes of ~100 mV and duration of 1–500 ms (long APs for recording from cardiomyocytes).

To acquaint the reader with the basic terminology used in the field and as a technical introduction we begin the discussion by describing the structural and electrical relationships formed between neurons and substrate-integrated MEAs and briefly explain the contribution of the various parameters to the electrical coupling between excitable cells (neurons and cardiomyocytes) and MEAs. We then review the micro- and nanoengineering approaches recently used in attempts to merge the benefits of extracellular MEAs with those of the sharp glass electrodes, as well as the critical problems that would have to be addressed in order for the new approaches to be incorporated in basic research and clinical applications. On the basis of this discussion we propose a tentative recipe that we believe might provide an optimal approach to construct an MEA that can provide simultaneous, long-term, multisite, non-destructive intracellular recording and stimulation of neurons.

Electrical circuit analogue of the neuron/electrode interface

The structural relationships between a neuron and a substrate-integrated planar electrode along with the analogue electrical circuit are schematically depicted in Fig. 1. The neuroelectronic hybrid is composed of three components (a) a neuron, (b) a cleft formed between the neuron and the substrate surface, and (c) the electrode.

Typically, differentiated neurons are non-isopotential structures with a cell body from which neurites in the form of a dendritic tree and a single long cylindrical axon emerge. These neuronal compartments adhere to MEA substrates by electrostatic or chemical interactions between adhesion molecules that protrude from the lipid membrane of the neurons and molecules deposited on the MEA platforms by the experimentalist[18,35]. The cleft formed between the cell membrane and the MEA substrate is filled with the ionic solution.

For the simplified model depicted in Fig. 1, the neuron surface area is subdivided into: a junctional membrane that faces the sensing pad(s) (with R_j as the junctional resistance), and the non-junctional membrane (with R_{nj} as the non-junctional resistance) that faces the bathing solution and the substrate. Propagating APs or synaptic potentials produce complex extracellular current flow between activated compartments and other parts of the neuron. Fractions of these extracellular currents flow between the non-junctional and the junctional membranes. The cleft, formed between the neuron and the sensing element, generates a resistance that is referred to as the seal resistance (R_{seal}). The voltage formed over R_{seal} directly modulates the gate voltage of a field-effect transistor (FET), or the charge dispersal across a passive metal electrode[36–38].

Neuron–device electrical coupling

The electrical coupling between a neuron or a cardiomyocyte and a sensing pad is defined here as the ratio between the maximal voltages recorded by the device in response to the maximal voltage generated by an excitable cell. Figure 2 illustrates how individual parameters of a passive analogue electrical circuit contribute to the coupling coefficient of slow membrane oscillations, medium-frequency synaptic potentials, and fast APs (Fig. 2a). The parameters used for the simulation approximate the passive physical properties of an excitable cell cultured on a substrate-integrated electrode (Fig. 2a).

Simulation of voltaic events of various frequencies illustrates that the coupling coefficient for higher-frequency APs is attenuated more strongly compared with postsynaptic potentials and membrane oscillations (Fig. 2b and Fig. 3).

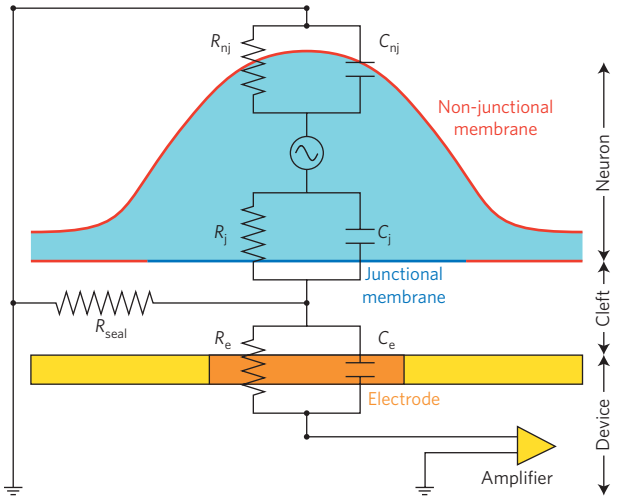

Figure 1 | Schematic layout depicting the spatial relationships between a neuron and a substrate-integrated electrode and the analogue passive electrical circuit. The cell body of a neuron (light blue) resides on a sensing electrode (orange) integrated in the culture substrate (yellow). The electrode is coupled to an amplifier (yellow). A cleft filled by the culturing media (ionic solution) interposes between the cell membrane and the electrode–substrate. The neurons plasma membrane is subdivided into two: the part that faces the electrode (blue) is defined as the junctional membrane and is represented by the junctional membrane resistance (R_j) and the junctional membrane conductance (C_j). The rest of the membrane, defined as the non-junctional membrane (red), faces the bathing solution and the culture substrate. This part of the membrane is represented by the non-junctional resistance (R_{nj}) and the non-junctional capacitance (C_{nj}). The physiological solution within the cleft generates the seal resistance (R_{seal}) to ground. The electrode (orange) impedance is represented by the electrode resistance and capacitance (R_e and C_e, respectively). The electrode can be a passive element or a transistor. For simulation purposes of APs or intracellular current injections, current can be injected into the analogue cell-circuit in-between R_{nj} and R_j. Under physiological conditions current is generated by transient changes in the membrane conductances. The colour coding shown here is used in Fig. 4 to depict the different components of the analogue electrical circuit.

Theoretical and experimental considerations revealed that reductively, the amplitude and shape of the FPs are determined by the multiplication of the R_{seal} value by the current that flows across it (Fig. 2c). For these reasons, intensive efforts were devoted to increase the value of R_{seal} (refs 35,37,39). Most of these research efforts yielded only limited improvements in the signal-to-noise ratio of the various devices. Studies of cell/electrode interfaces showed typical cleft thicknesses between 40–100 nm (refs 40–44). For most cell types this would correspond to R_{seal} in the range of 1–2 MΩ and FP recordings in the range of a few tens to few hundreds of microvolts.

Another factor that largely affects the electrical coupling coefficient between cells and an MEA is the input impedance of the sensing pad (Fig. 1 and Fig. 2d). The currents of living cells and electronic devices are fundamentally different: the former are formed by ions in solution whereas the latter, by electrons in mostly solid-state metals and semiconductors[37,45]. The ramification of this difference is the effect of the impedance of the device on the electrical coupling, reflected by the sensing pad geometry and the material it is composed of. Typically the impedance of the sensing pad, either constructed from noble metals or insulated semiconductors, is attributed to the 'blocking' ion bilayer formed at the device

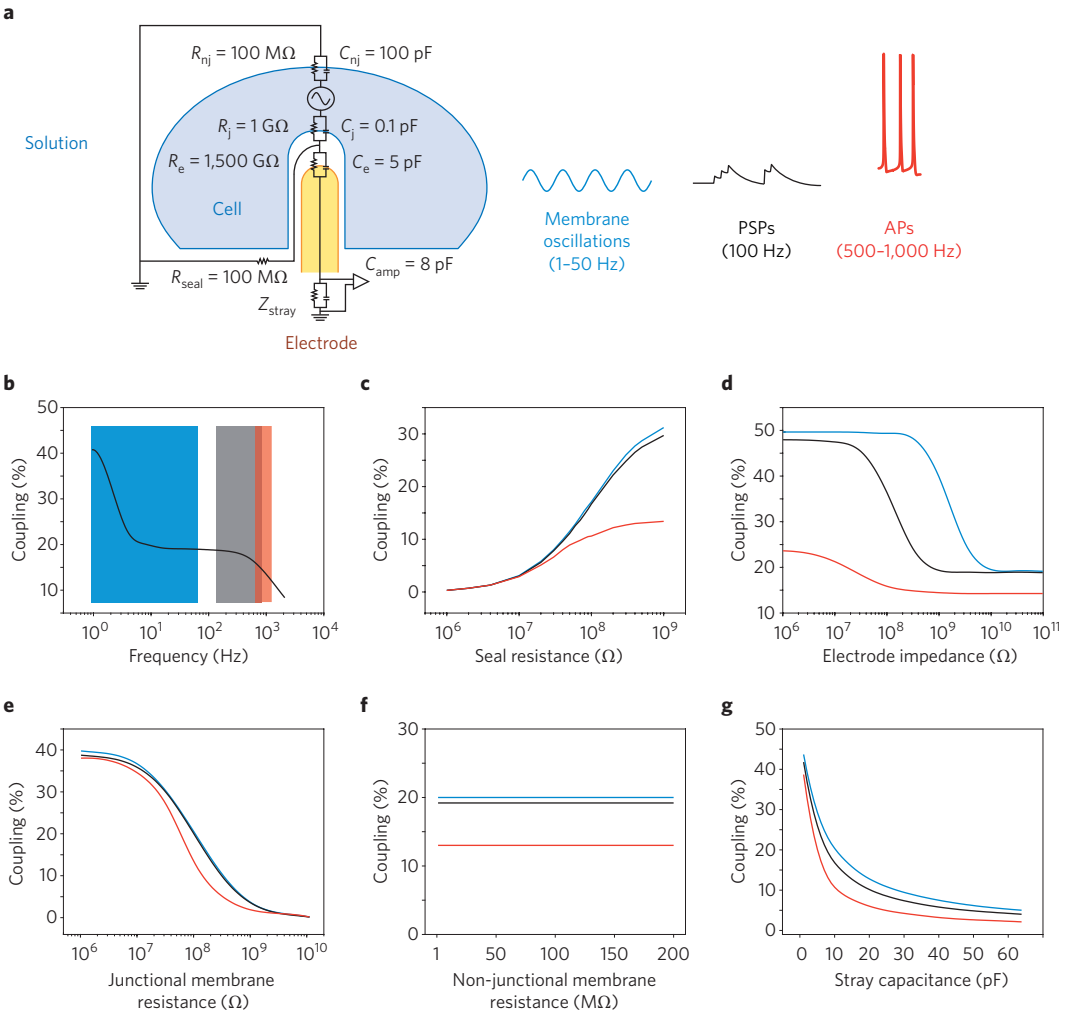

Figure 2 | Simulation of the contribution of individual electrical components to the neuron-electrode electrical coupling coefficient. a, Left: the analogue passive electrical circuit and default parameters used for the simulation parameters of a representative passive analogue electrical circuit. Right: the simulations were conducted for low-frequency signals depicting membrane oscillations, medium frequencies depicting postsynaptic potentials (PSPs) and fast frequencies depicting APs. C_{amp}, input capacitance of the amplifier; Z_{stray}, stray impedence. For the simulation, all default parameters were kept constant as shown in (**a**) while the tested parameter was varied in the range indicated by the horizontal axis. **b**–**g**, The coupling coefficient as a function of: voltage pulse frequency (**b**), the seal resistance (**c**), the sensing pad impedance (**d**), the junctional membrane resistance (**e**), the non-junctional membrane resistance (**f**) and the stray capacitance (**g**). Simulations based on refs 64,65.

active region and the ionic solution in which the neurons reside. For example, standard planar gold electrodes with radius of 30 μm have impedances of 50 KΩ at 1 KHz in electrolyte solution. Reducing the surface area of individual sensing pads to match the dimensions of individual neurons enables the density of the MEA and its spatial resolution to be increased[5,7,8,46,47]. This however, is reflected by the reduction of the FP amplitudes as a result of the increase in impedance and consequent reduction of the signal-to-noise ratio. Thus, the electrodes geometry and the ensuing impedance both place constraints on reducing the electrode size. Increasing the surface area by using nanostructures such as spongy platinum black or Ti_3N_4 (refs 48–50), gold nanoflakes and nanopillars[51,52], or carbon nanotubes[53,54] is used to compensate for the dimensions of the electrode surface 'visible' to the cell. Although effective in reducing the impedance values up to 95% at approximately 1 KHz (ref. 54), in practice the recorded FPs are still in the range of hundreds of microvolts. This is most likely due to averaging of the complex positive and negative currents concomitantly generated by a number of sources, over fractions of the large surface area of the electrode. This 'averaging' usually results in reduced amplitude of the electrical readout. It should be noted, however, that reduction of the electrode impedance may be very effective in improving the readout signals when applied under conditions in which a single cell 'covers', engulfs or internalizes a single electrode such as those described in this Review (Fig. 4).

The junctional membrane is defined as the resistance and capacitance of a membrane patch that faces the sensing pad or the gate of an FET (Fig. 1). The surface area of the junctional membrane can be anywhere between a very small fraction of the cell surface area, up to approximately 50% in cells that flatten while adhering strongly to substrate-integrated sensing pads. This variable depends on the geometry of the sensing pad and the morphology and adhesion characteristics of the specific cell. The junctional membrane can thus be of very high resistance and low capacitance. This implies that only a small fraction of the current generated across the neuron's membrane, flows through the junctional membrane. Reduction of the junctional membrane resistance would be very effective in improving the electrical coupling coefficient between a neuron and an electrode (Fig. 2e and Fig. 3). This is in fact the approach used by the classical methods of sharp electrodes, whole-cell patch electrodes or the perforated

patch configuration[3,55] (Fig. 4a,b). Attempts to improve the electrical coupling coefficient between cultured cells and planar MEAs by expression of ion channels in the plasma membrane provided experimental demonstrations of the contribution of the conductance of the junctional membrane[37]. Nevertheless, experimental manipulation to improve the electrical coupling by expression of ion channels in neurons should not be used in studies of neuronal networks as such a manipulation changes the electroanatomy of the cells and their excitability and thus alters the functioning of the network being studied. In some recent studies, local increases in the junctional membrane conductance by localized electroporation have been used to transiently increase the coupling coefficient[56–60] (Fig. 4e).

Unavoidable stray capacitance along the conducting lines, together with the input impedance of the amplifying circuitry, further attenuates the recorded signals (Fig. 2g).

Recently, a number of laboratories began to merge the advantages of extracellular MEAs and intracellular microelectrodes. In the following paragraphs we describe the novel approaches, identifying their strengths and limitations from the point of view of the end users.

Neurons actively engulf protruding electrodes

The first series of studies reporting on successful multisite, non-invasive, intracellular recording and stimulation by MEAs were published by our laboratory between 2007 and 2010[61–65]. In these studies we increased the neuron–microelectrode electrical coupling coefficient from approximately 0.1% as recorded by a planar extracellular MEA to approximately 50% by the use of a chemically functionalized micrometre-size mushroom-shaped gold protrusion as the sensing electrode (Fig. 4d and Fig. 5a). The increased coupling coefficient was associated with an intracellular recording of a monophasic positive attenuated intracellular AP instead of a typical biphasic FP. The unique neuron–electrode configuration used in this work, made it possible, for the first time, to record with a MEA action potentials as well as synaptic potentials (Fig. 5c). The key to the multi-electrode-array 'in-cell recording' approach developed by us is the outcome of three converging cell biological principals: (a) the activation of endocytotic-like mechanisms in which cultured *Aplysia* neurons are induced to actively engulf gold mushroom-shaped microelectrodes (gMμE) that protrude from a flat substrate, (b) the generation of high R_{seal} between the cell's membrane and the engulfed gMμE, and (c) the increased junctional membrane conductance.

The neuron/gMμE interface was generated by chemically 'luring' the neurons to engulf the protruding gMμE by a highly conserved cell biological mechanism — endocytosis (which is a cell biological mechanism that underlies the internalization of particles into the cells[66]). The shape and the dimension of the gMμE were selected to mimic the geometry and dimensions of dendritic spines[67]. To facilitate the engulfment, the gMμEs were chemically functionalized by an RGD-based peptide[35]. This is one of a group of well-known molecular recognition motifs that trigger adhesion and engulfment mechanisms[68]. The localized presentation of the peptide by the gMμE (and possibly the electrode geometry itself) led to active engulfment of the electrodes by *Aplysia* neurons and a number of cell lines[61–65]. The engulfment of the microelectrodes is generated by molecular cascades that include the restructuring of the cytoskeleton to form an actin ring around the stalk of the 'gold mushroom' (Fig. 4d and Fig. 5a, left panel).

Using biophysical parameters obtained by direct measurements of the non-junctional resistance, non-junctional capacitance, electrode resistance, electrode capacitance and R_{seal}, as well as the estimated value of the junctional membrane properties calculated according to the geometry of the gMμE (Table 1), we simulated the expected recordings of APs and subthreshold potentials using an equivalent electrical circuit. We found that the calculated values used for the junctional resistance were insufficient to generate the neuron–electrode coupling coefficient as that obtained

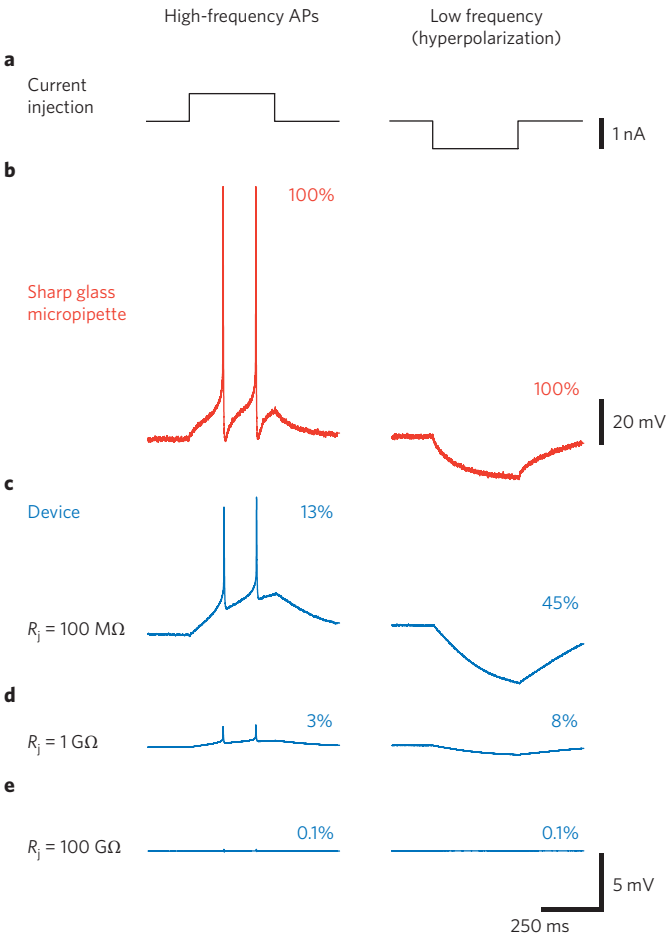

Figure 3 | Dependency of the electrical coupling on the junctional membrane resistance and pulse duration. Shown is a simulation of the cell–device coupling of APs and a long hyperpolarizing pulse at three different values of R_j (100 MΩ, 1 GΩ and 100 GΩ) **a**, Schematic illustrations of the depolarizing (left) and hyperpolarizing current pulse (right) delivered to generate two APs and membrane hyperpolarization, respectively. **b**, Simulation of the ensuing intracellular potentials recorded by an intracellular electrode (red). **c**–**e**, The recorded potentials by an extracellular-located electrode (as shown in Figs 1 and 2) under different junctional membrane values (blue). Note that the amplitude of the extracellularly recorded APs (short pulses) is reduced faster than the voltage generated by the long pulse. That is, the coupling coefficient of the AP is more sensitive to the value of R_j than that of the long pulse. The values used for the simulation are identical to those shown in Fig. 2 although R_j is altered as indicated.

experimentally. To reach the coupling level observed in the experiments we had to increase the junctional membrane conductance by at least an order of magnitude[64,65]. The mechanism underlying the increased junctional membrane conductance is not known. It is conceivable that in association with the cytoskeleton restructuring around the gMμE, voltage-independent ion channels are recruited to the junctional membrane to sufficiently increase the junctional conductance without leading to noticeable effects on the passive and active membrane properties. An alternative explanation could be that the mechanical tension generated at the curvature of the gMμE generates non-specific membrane nanopores[58,69]. An important question that was brought up in this relation is whether the growth of *Aplysia* neurons on a matrix of gMμEs is altering the neuron's physiological properties. We found that the growth of the neurons on gMμEs did not alter the biophysical properties of the neurons

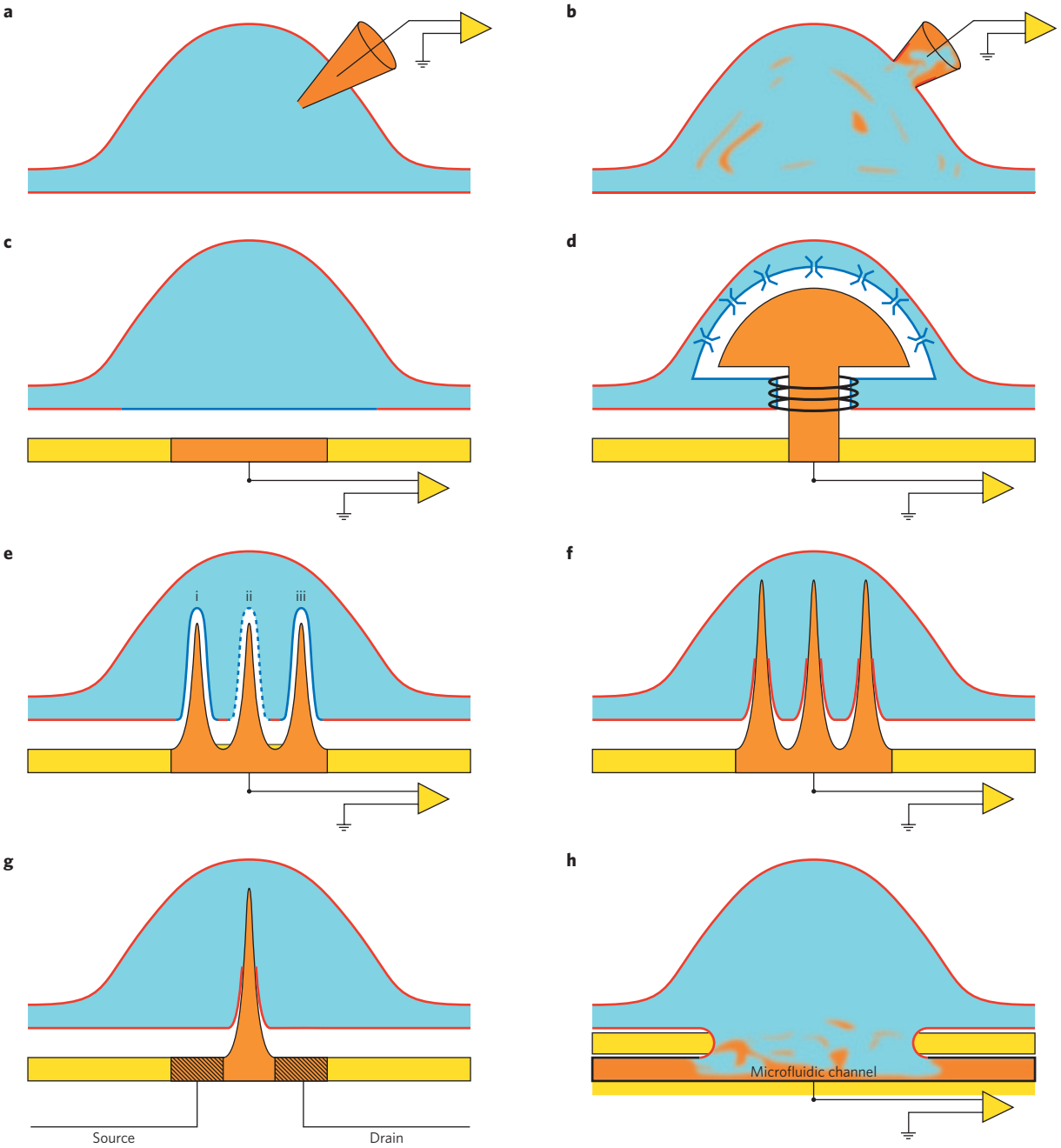

Figure 4 | Different forms of the electrode/neuron interface configuration. The colour code represented here for the different components is the same as for Fig. 2. **a**, A sharp glass intracellular microelectrode. **b**, Whole-cell patch-electrode configuration. The 'mixing' of orange and blue schematically illustrates the perfusion of the cytosol by the electrodes content. **c**, A neuron cultured on a substrate-integrated planar extracellular electrode. Note the cleft (white) separating the junctional membrane and the electrode. **d**, A neuron engulfing a gold mushroom-shaped protruding microelectrode. Note actin rings surrounding the mushrooms stalk stabilizing the configuration. **e**, Nanopillar electrodes extending into a cultured cardiomyocyte but that do not penetrate the plasma membrane (i). After the application of an electroporating pulse (ii) the nanopillar gains access to the cytoplasm. The electroporation is transient and the junctional membrane resistance recovers to control level within minutes (iii). **f**, An array of nanopillars that penetrate the plasma membrane forming direct physical contact with the cytosol. **g**, A nanopillar that serves as the gate for a nano-FET penetrates the cell's membrane. **h**, Patch clamping of cultured neurons. The mixing of the ionic solution of the microfluidic system with the cytosol is depicted. For more details see main text.

or their synaptic communication. It does however alter the typical growth patterns of the neurites[63].

Stimulation of cells by substrate-integrated electrodes (either passive metal electrodes or FETs) often involves undesired electrochemical reaction products at the electrode interface and consequently damage to the cells that goes beyond transient electroporation. Measurements of the neurons input resistance before and after stimulation by gMμEs showed no change, affirming that high enough charge transfer can be applied to evoke APs without damage to the cell[64].

Out of the five criteria to evaluate of the benefits of the approaches, the gMμE-based MEA provided multisite, simultaneous, intracellular recording and stimulation for periods of days (which is for as long as we carried out the recordings). The filtering properties of the gold electrodes and the a.c. amplifier used do not enable the resting potentials of the neurons to be recorded. Nevertheless, the configuration

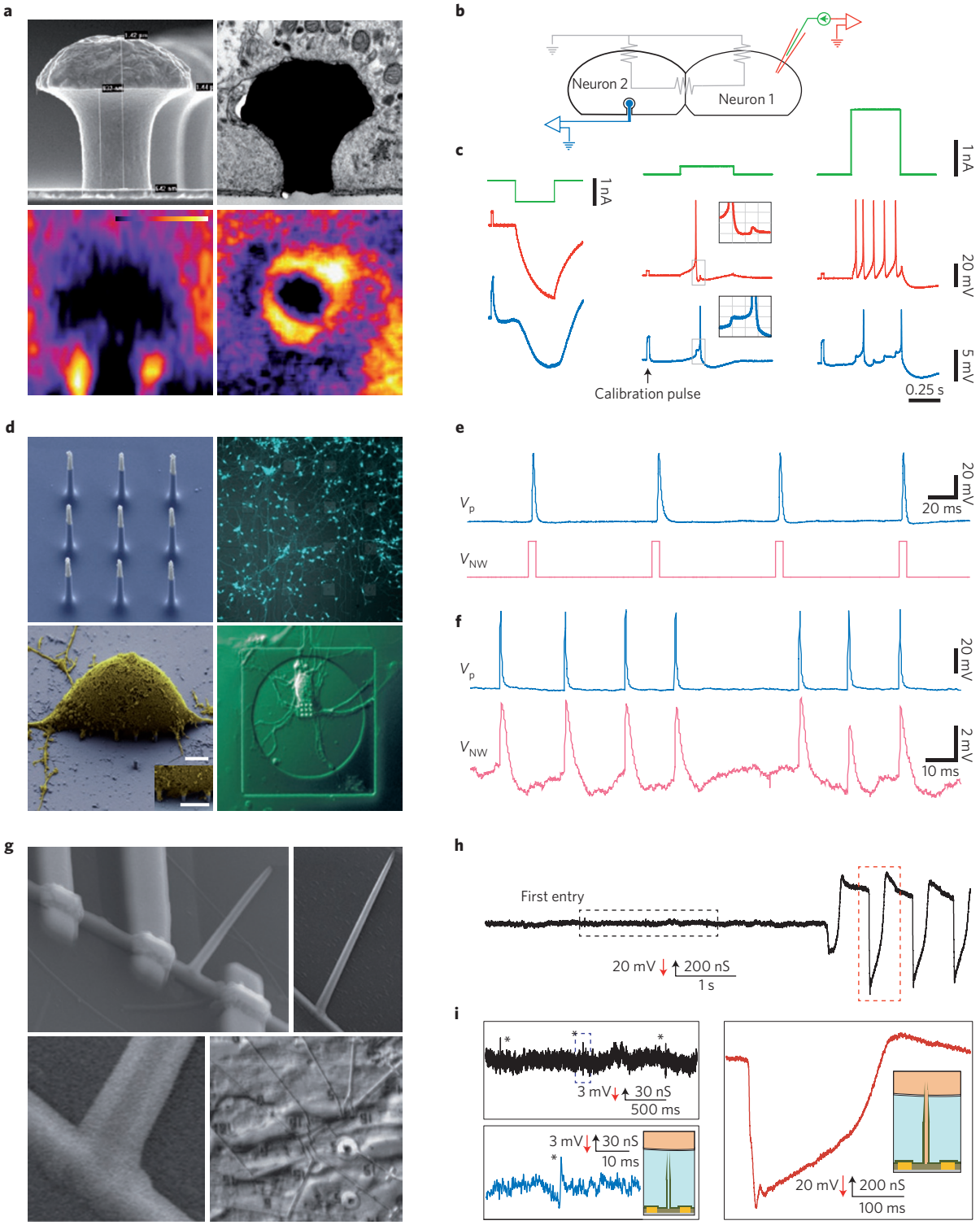

Figure 5 | Recently developed MEA devices record intracellular potential from excitable cells. a, Gold mushroom-shaped microelectrodes (gMμEs) functionalized with RGD-based peptide (top left, scanning electron microscopy (SEM) image) are engulfed by *Aplysia* neurons (top right, transmission electron microscopy image), which induces cytoskeletal reorganization around the structure (bottom, confocal microscopy images). The gMμE is 1.42 μm high. **b**,**c**, Stimulation and recording of APs and subthreshold synaptic potentials is achieved by the gMμEs with a signal-to-noise ratio similar to sharp-glass and patch-clamp micropipettes. Green, current injection into the neuron; red, intracellular recording by a glass microelectrode; blue, in-cell recording by an extracellular gold mushroom microelectrode. **d**, SEM (left) and optical (right) images of vertical nanowire electrode arrays (VNEAs). Scale bars, 2.5 μm. **e**,**f**, Vertical nanowire electrode arrays (VNEA) can stimulate (**e**) and record (**f**) from rat cortical neurons monophasic APs. V_p, patch clamp voltage; V_{NW}, nanowire recordings voltage. **g**–**i**, A phospholipid-functionalized silicon nanotube as the gate electrode of an FET device records APs from cardiomyocytes with a signal-to-noise ratio similar to glass electrodes. **g**, SEM images of the device (left) and of cardiomyocytes grown on it (bottom right). **h**, Recording from a nanotube before peneration (left) of the cell's plasma membrane and after penetration (right). **i**, Left: FPs recorded by the nanotube before penetration of the cell. Right: a single intracellularly recorded potential. Figure reproduced with permission from: **a**, Top: ref. 62, © 2009 RSC; Bottom: ref. 63, © 2009 IOP; **b**,**c**, ref. 64, © 2010 Am. Physiological Soc.; **d**–**f**, ref. 71, © 2012 NPG; **g**–**i**, ref. 78, © 2012 NPG.

Table 1 | Methods for recording and stimulation of electrogenic cells.

	Seal (Ω)	Maximum AP (mV)	Maximum EPSP (mV)	Cell type studied	Coupling coefficient	Duration of stable recording	Electrode impedance (Ω)	Primary electrode material	Insertion method	Coating	Ref.
Sharp-glass electrodes	10^8	*	*	Multiple	1	Hours	10^6	Glass micropipette	Mechanical	None	4
Patch-clamp electrodes (whole cell)	$>10^9$	*	*	Multiple	1	Hours	10^6	Glass micropipette	Mechanical	None	3
Planar MEA and transistors arrays	10^6	<1	None	Multiple	0.001–0.01	>months	10^5 cm^{-2}	Metals	None	Multiple	45
Gold mushroom-shaped MEA (gMμE)	10^8	25	5	Neurons (*Aplysia*)	~0.5	>2 days	10^{11}	Au	Biological endocytosis	RGD motif peptide	64
Kinked silicon-nanowire FET	N/A	80**	None	Cardio-myocytes	~1	Seconds	Irrelevant (FET device)	Si	Mechanical or spontaneous	Phospho-lipids	77
Vertical nanowire electrode arrays (VNEA)	$>10^8$	4	None	Neurons (cortical rat)	~0.3	10 min	3×10^8 (with application of bias voltage = 1.5 V)	Si with Au tip	Bias voltage	Silanization	71
Branched intracellular nanotube-FET	N/A	75–100	None	Cardio-myocytes (embryonic chicken)	~1	1 h	Irrelevant (FET device)	Si	Mechanical or spontaneous	Phospho-lipids	78
Nanopillar electroporation	N/A	12	None	HL-1 cell line	~0.1	10 min per daily session, 3 days	6×10^6 to 18×10^6 (depending on the number of pillars)	Pt	Electroporating current	Fibronectin	57
gMμE electroporation	10^8	6	None	Neurons (*Aplysia*)	~0.1	5 min	10^{11}	Au	Electroporating current	Poly-L-lysine	58
Active silicon nanotube transistor	N/A	80	None	Cardio-myocytes (embryonic chicken)	~1	N/A	Irrelevant (FET device)	Si nanotube	Mechanical or spontaneous	Phospho-lipids	84

Electrical and methodological specifications of the available modalities of cellular electrical recordings: from sharp-glass and patch-clamp electrodes to planar microelectrode and FET arrays and through to the recently developed intracellular-recording nano- and microdevices. *Glass micropipettes provide maximal (one-to-one) AP and EPSP amplitudes. ** Estimated from conductivity change.

successfully monitored subthreshold synaptic potentials and APs (Fig. 5c, middle panel). The filtering nature of the recording system can be deconvoluted and thus unfiltered high-quality recordings of APs and synaptic potentials can be retrieved. A stable electrical coupling between gMμE and a neuron coincided with the formation of cytoskeletal actin rings surrounding the stalks of the mushroom-like structure[59,63] (Fig. 5a, lower panel). Individual gMμE enables both voltage recordings and application of current[64]. So far, attempts to obtain in-cell recordings and stimulation from rat hippocampal neurons and primary cardiomyocytes were unsuccessful. It should be noted nevertheless that these attempts were limited to gMμE functionalized with poly-D-lysine rather than by the engulfment promoting peptide.

Nanopillars for intracellular recordings and stimulation

Sharp glass electrodes (Fig. 4a) and patch electrodes (Fig. 4b) provide excellent intracellular recording by penetrating the plasma membrane and directly accessing the cytosol while generating effective R_{seal} with the plasma membrane (hundreds of MΩ to a few GΩ, respectively, Table 1). A recent study from Park's laboratory[71] used vertical nanowire electrode arrays (VNEAs) constructed from a doped silicon core encapsulated by silicon dioxide and tipped by Ti/Au, to generate an identical configuration to sharp intracellular electrodes (Fig. 4f and Fig. 5d). In the study, 3 × 3 arrays of 9 nanopillars, 150 nm in diameter, 3 μm in height at 2 μm pitch were grown on 16 sensing pads. Embryonic rat cortical neurons or HEK293 cells were then cultured on the VNEAs for a number of days. About 50% of the VNEAs spontaneously penetrated through the plasma membrane of the HEK293 cells as demonstrated by the fact that current injection through the VNEAs generated a voltage drop across the plasma membrane. In cases where spontaneous penetration of the membrane was not evident, an electroporating pulse (approximately ±6 V, 100 ms) was applied to penetrate the membrane of the neuron. The effect of the electroporating pulse on the integrity of the membrane was not shown. The seal resistance formed between the VNEAs and the plasma membrane was estimated to be 100–500 MΩ. The VNEAs were used in two regimes: in the Faradic regime, when a bias of ~−1.5 V was applied to the nanowire and the access resistance was reduced to 300 MΩ, and in the capacitive regime, when no bias was delivered and the access resistance was infinite. Accordingly, in the Faradic regime the electrical coupling for APs between the cell and the VNEA was about 10% whereas in the capacitive regime the attenuation was larger, reaching a lower coupling of ~0.1–0.3% (Table 1).

Consistent with the intracellular positioning of the VNEA, all recorded APs were positive monophasic (as discussed in refs 18,70). However, the coupling coefficient and signal-to-noise

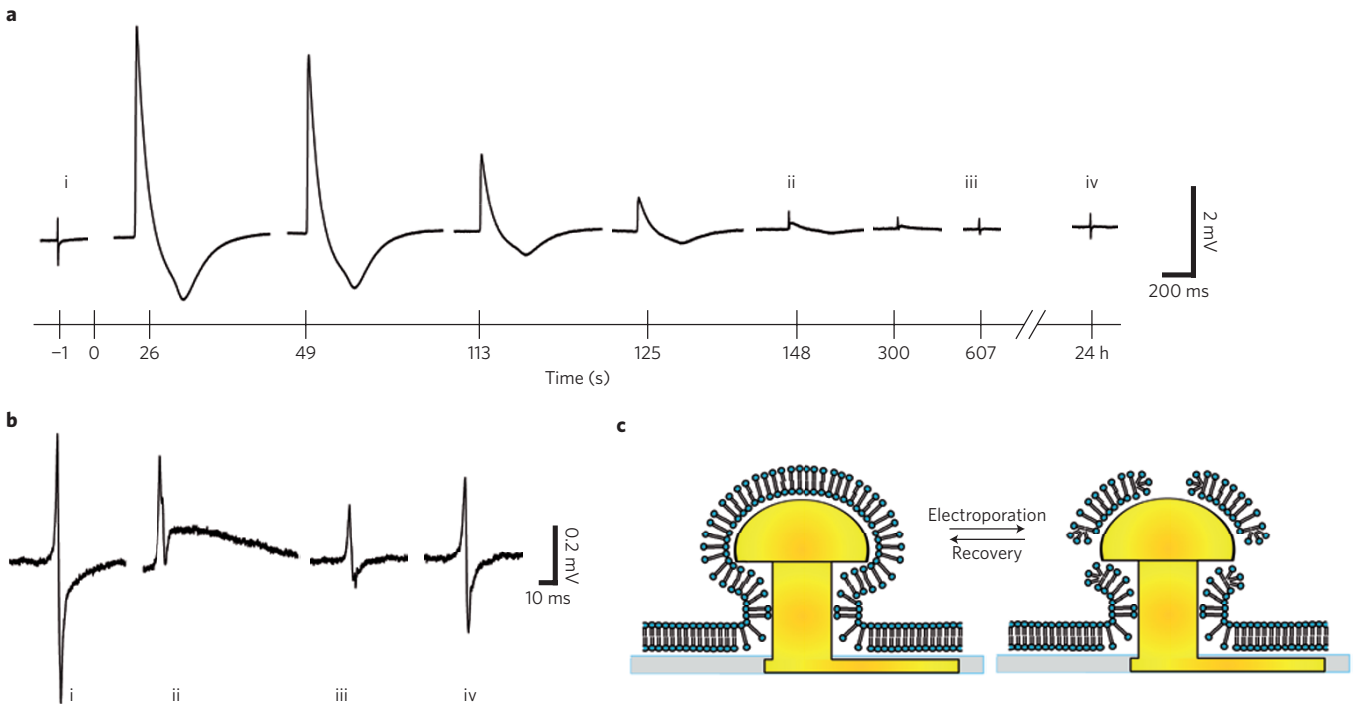

Figure 6 | From extracellular field-potential recordings to intracellular recordings and the recovery process. a, Before electroporation, a gMμE recorded a rat cardiomyocyte extracellular FP (**a**, (i); enlarged in **b**, (i)). After the delivery of an electroporating pulse (100 ms, 1 V) (at 0 s) the biphasic FP transformed into a monophasic 5 mV positive potential with a shape similar to that reported by intracellular recordings. The amplitude of the AP diminished over time 125–148 s, gradually resuming the shape of the extracellular FP after electroporation. Thereafter the shape of the FP gradually recovered (between 148–607 s, enlarged in **b**, i–iv) regaining the typical biphasic shape (**a**, (iv) and **b**, (iv)). **b**, Enlargements of the FPs before electroporation (i) and 148 s (ii), 607 s (iii) and 24 h (iv) after electroporation. **c**, Schematic drawing of the presumed reversible effects of an electroporating pulse on the plasma membrane facing a gMμE. Figure reproduced with permission from ref. 59, © 2012 Frontiers Media.

ratio were insufficient to enable recordings of subthreshold synaptic potentials. In fact, in relation to the five examination criteria listed above, the recordings obtained by the VNEA do not provide significant advantages over extracellularly positioned gMμE in cultured hippocampal neurons[70]. The relatively low coupling coefficient of the VNEA-based sensor is most likely due to the high impedance of the VNEAs (Table 1). An advantage of recording by VNEAs over recordings by classical substrate-integrated planar electrodes (but not small electrodes[7]) is that a single pad records APs from an individual neuron. Although Robinson *et al.*[71] emphasize the usefulness of VNEAs to address individual neurons by electrical stimulation and record the ensuing synaptic potentials by a patch electrode, it should be noted that different types of extracellular micrometre-size planar (Fig. 4c) and protruding microelectrodes have been shown to effectively record or stimulate single cells[19,56,72,73]. For example, Hofmann *et al.*[73] constructed a liquid-filled nanocavity (50 nm in height) that accesses a low impedance electrode by the fluid that fills the cavity. The functional contact of a cell with the electrode is through an aperture with a diameter smaller than the cell's. This configuration increases the spatial resolution of a MEA and increases the R_{seal} formed between the cell and the device. The cell–nanocavity configuration enables negative almost monophasic FPs with amplitudes >1 mV to be recorded. Using an array of 600-nm-thick tungsten protruding micronail-like electrodes Huys *et al.*[19] recorded biphasic or monophasic negative FPs of 50–100 μV. These micronails also enabled single cells to be stimulated effectively.

Intracellular recordings by membrane electroporation

As pointed out by Robinson *et al.*[71], only a fraction of the nanowires spontaneously penetrate the plasma membrane. Nevertheless, application of current through the pillars readily leads to their functional penetration.

Four recent studies demonstrated for the first time that localized membrane electroporation may lead to transient intracellular recordings of attenuated APs. Xie *et al.* demonstrated electroporation of cultured cardiomyocytes by vertical nanopillar electrodes[57], Hai and Spira[58], and Fendyur and Spira[59] demonstrated electroporation of cultured *Aplysia* neurons and primary cultured rat cardiomyocytes, respectively, by the gMμEs, and Breaken *et al.* demonstrated single-cell cardiomyocytes electroporation using micrometre-sized TiN protruding electrodes[60]. In all four studies the intracellular access was transient suggesting that electroporation activates repair mechanisms that seal off the electroporated nanopores[58], leaving the protruding nano- or microelectrodes out of the cell (Fig. 6). In these studies, the electroporating pulses reduced the junctional membrane resistance sufficiently to transform a typical biphasic cardiomyocyte FP to a 1–11 mV positive monophasic AP. The shape of the attenuated AP was typical of cardiomyocyte potentials.

The transient nature of the electrical coupling and the attenuation of the APs indicate that electroporation cannot be the method of choice to improve the quality of the interface formed between micro- or nano-based MEAs and the cell's membrane. Nevertheless, as it was demonstrated by the Melosh laboratory[74–76] and already applied by the Lieber laboratory[77,78], it is conceivable that membrane–electrode fusion and GΩ seal formation can be facilitated by proper surface functionalization of the electrodes using lipid-based agents.

It is of interest to note that the nanopillar approach does not provide a significant advantage over planar extracellular electrodes as the recorded potentials are attenuated by at least an order of magnitude by the inherent high electrode impedance and the insufficient R_{seal}. It should also be noted that even if a single sensing pad carries

multiple nanopillars, and a number of them penetrate the plasma membrane, the electrodes impedance is too high to enable recording of subthreshold potentials[57,71] (Table 1). Theoretically, the impedance problem could be solved by increasing the density of the nanopillars over the sensing pad. Nevertheless, when the density of protruding nanostructures exceeds a certain bound, the pillars do not penetrate the cell membrane, analogous to a dense 'bed of nails'. For example, Bruggermann *et al.* fabricated densely packed vertical (60 nm diameter, 300–400-nm-high) gold pillars on 15-μm-diameter pads[52]. In spite of the nanometric dimensions of the pillars, spontaneously firing HL-1 cells cultured on the MEA generated large ~1 mV negative monophasic FPs. This clearly pointed out that the pillar nanoelectrodes maintained an extracellular position. In a similar manner, densely packed (2 μm pitch) micronail-shaped structures record low amplitude (~100 μV) biphasic or negative-monophasic extracellular FPs from cultured rat cardiomyocytes[79]. In conclusion, although physical contact between a nanoparticle and the plasma membrane may be sufficient to induce particle penetration through the plasma membrane[80], higher-density nanocontacts (aiming at lowering the electrode impedance) may prevent membrane penetration from occurring. Thus, optimization of the pillar number, to reduce the impedance and pillar densities to promote internalization is critical.

Overcoming the constraints of nanopillar impedence

Using advanced semiconductor-based nanotechnology and the classical concepts of mechanically penetrating the cell plasma membrane by sharp glass microelectrodes, Lieber's laboratory demonstrated intracellular recordings of 80–100 mV APs from beating cultured cardiomyocytes (Fig. 5g). This was done either by the so-called kinked nanowires[77] or pillar-shaped protruding silicon nanowires[78], nanofabricated as the sensing gate electrode of an FET.

In the work described by Tian and Cohen-Karni *et al.*, an FET was generated at the tip of an ~80 nm kinked silicon nanowire by way of *in situ* doping[77]. In the work described by Duan *et al.* a protruding silicon nanowire was integrated onto the gate of the FET[78] (Fig. 5g). To facilitate the penetration of the electrodes into the cells the device's surface was modified by phospholipids[77]. Spontaneous fusion of the applied phospholipids with the lipid membrane of the cells seems to underlie the formation of the GΩ seal. Using both types of nanosensors, full blown cardiac APs of 75–100 mV, ~200 ms were recorded (Fig. 5h,i). The high-quality measurements of the APs were made possible by three factors: (a) the nanoscale size of the sensors that enabled its insertion into the cytosol through the plasma membrane of the cells, (b) the formation of GΩ resistance between the plasma membrane and the nanostructures, (c) the fact that the size of the sensing area does not affect its sensitivity[78,81,82]. It should be noted that whereas the aspects of nano-dimensions and GΩ seal formation are essential components to enable high-quality recordings, the key to the success is the use of the gate electrode of an FET as the sensing electrode rather than passive metal or silicon-based micro- or nanoelectrodes. Thus, in contrast with passive conducting lines, where the signal is significantly attenuated due to stray capacitance, an FET effectively amplifies the signal *in situ*. It should be noted that FETs are more susceptible to failure due to leakage currents, whereas passive electrodes are not affected as dramatically by device imperfections.

The approach used by Lieber's laboratory to insert the nanopillars into the cells[77,78,83,84] was to transfer a layer of 'mature' cardiomyocytes grown on a thin piece of polydimethylsiloxane, upside down, onto the device surface and apply gentle downward pressure onto the substrate. This manipulation led to the insertion of the nanoelectrodes into the cells within approximately 45 s. Whereas at the 'proof-of-concept' level the approach taken by Lieber's laboratory is sufficient, it should be further developed to enable experiments in which cardiomyocytes and neurons can be cultured and grown in continuous contact with the MEA substrate and maintain the cells–electrodes contact for long periods rather than be acutely manipulated.

When considering the branched intracellular nanotube-FET or kinked nanoelectrode devices as tools to map functional synaptic connectivity, a major hurdle is the signal-to-noise level of the device. Examination of some recordings (for example, see Fig. 4 in ref. 78) reveals noise levels of more than 20 mV. Whereas the noise is attributed to the nano-dimensions of the FETs and thus can be reduced by adjusting the FET size, the present device does not provide the resolution to enable the recording of miniature potentials, synaptic potentials and small membrane oscillations. Another unsolved problem that would need further study is to enable the accurate recordings of the resting potentials.

Planar patch-clamp MEA technology

Another line of investigation to overcome the problems of high junctional membrane resistance, electrode impedance and of low R_{seal} revolves around microfluidic-based MEAs able to patch clamp neurons under *in vitro* conditions. The approach is extensively used to acutely patch cells in suspension relying on suction to draw individual cells to the aperture and to form a giga-seal resistance. Thus far the approach was not suitable for studies of long-term adhering cultured neuronal networks[85,86]. Recently Martina *et al.*[87] began demonstrating that the approach has a potential to be adapted to neuronal networks. In this study a silicon oxide substrate or silicon oxide laminated by polyimide film containing 2 to 4-μm-sized apertures were used. Each aperture was connected to a microfluidic channel. Two isolated cell bodies of identifiable *Lymnaea* neurons were co-cultured over the apertures for 8–12 h. Within this time the cell bodies formed chemical synapses and adhered to the substrate to spontaneously form an unusually high GΩ seal resistance. Negative pressure pulse through the microfluidic system broke the junctional membrane establishing a classical whole-cell patch-clamp configuration. In a fraction of the experiments the patch configuration was stable for a number of hours and the properties of the synapses formed between the two cells could be investigated. The signal-to-noise ratio obtained by the planar patch-clamp device matches that of conventional patch-clamp recording. Although promising, it should be noted that the somata of the isolated neurons adhered to each other but did not extend neurites on the culture substrate. Thus the neuron–device configuration did not simulate the complex growth pattern of cultured mammalian neurons but rather is closer to the cell suspension mode of patch-clamp recordings.

When considering the potential use of planar patch-clamp MEAs as tools to map functional synaptic connectivity among cultured neurons, two major problems have to be dealt with: (a) the recording duration is expected to be limited by the perfusion of the neuron by the microfluidic solutions (Fig. 4h), (b) the sensor's density (apertures) is expected to be limited by the backside fluidic system.

Conclusions

On the basis of the results reviewed above and theoretical considerations, we estimate that nano- and micro-electrophysiological technologies enabling simultaneous, long-term, multisite, intracellular recording and stimulation from many neurons under *in vitro* and *in vivo* conditions will become available to the neuroscientist community within a number of years.

The approaches that at present reveal the best potential are: the bioinspired use of protruding electrodes that are engulfed by neurons, and the use of nanostructures that penetrate the plasma membrane in a similar way to classical sharp microelectrodes. Experimentations with passive nanopillar-based protruding structures functionalized by lipid layers revealed that whereas single or multiple nanopillars can penetrate the cell's plasma membrane forming relatively high R_{seal}, the high nano-electrode impedance/R_{seal} ratio value attenuates the recorded potential to a level that makes it impossible to record synaptic potentials or

subthreshold membrane oscillations. Attempts to reduce the electrode impedance by fabricating multiple nanopillars on a single sensing pad did not solve the problem[71]. It seems that increasing the number and density of the nanopillars to reach low enough impedance (and improve the electrode impedance/R_{seal} ratio) is limited by cell biological properties as cells cultured on high-density nanopillars do not extend the plasma membrane into narrow spaces between the pillars[52,79] and that physically inserting a dense population of nanopillars would be damaging to the cell. It is for these reasons that current passive nanopillar electrodes cannot be used as substitutes for traditional glass micropipette electrodes for intracellular recordings from neurons. Another severe limitation with the use of nanopillars is the instability of the intracellular configuration. So far, mechanisms to stabilize the intracellular positioning of the nanopillars have not been addressed.

On the other hand, the use of either kinked nanowires[77] or pillar-shaped protruding silicon nanowires[78], as the gate electrodes of an FET device, bypasses the problem of high electrode impedance (as FET recordings are independent of gate impedance[78,81,82]). Because of their nanoscale dimensions, the use of FET-based nanosensors can also enable the simultaneous recordings from subcellular compartments (dendrite, somata, axon, varicosities and others). The current limitations of the nanopillars–FET devices for intracellular recordings are: the inherent noise level of the nano-FETs, and the need to mechanically manipulate the cultured cells and the substrate on which they grow into physical contact with the electrodes. The problem of noise may be dealt with by modulating the transistor size and geometry[88] while taking into consideration the limitations of ambient thermal noise in electrolytic solutions[89]. The issue of having to mechanically press the cells and device to acutely form physical contact may be solved by merging some of the concepts developed by us and the Lieber laboratory.

So far, the gMμE-based MEA is the only device that enabled the recordings of both APs and subthreshold synaptic potentials, and that can also be used for effective intracellular stimulation[64]. Nevertheless, this coupling was demonstrated using large *Aplysia* neurons but as of yet has not successfully been applied to rat hippocampal neurons and primary rat cardiomyocytes.

It is conceivable that merging the cell-biological principles of evoking engulfment of the electrodes on the one hand and the use of FETs on the other may provide both a stable neuron–electrode configuration and intracellular access. Once achieved, such a device may be applied in arrays that make use of the well-established multiplexing capabilities of ultra-large-scale integrated transistor arrays.

Received 2 August 2012; accepted 18 December 2012; published online 5 February 2013

References

1. Hodgkin, A. L. & Huxley, A. F. Action potentials recorded from inside a nerve fibre. *Nature* **144,** 710–711 (1939).
2. Grundfest, H. The mechanisms of discharge of the electric organs in relation to general and comparative electrophysiology. *Prog. Biophys. Biophys. Chem.* **7,** 1–85 (1957).
3. Sakmann, B. & Neher, E. Patch clamp techniques for studying ionic channels in excitable membranes. *Annu. Rev. Physiol.* **46,** 455–472 (1984).
4. Verkhratsky, A., Krishtal, O. A. & Petersen, O. H. From Galvani to patch clamp: the development of electrophysiology. *Pflugers Arch.* **453,** 233–247 (2006).
5. Hutzler, M. *et al.* High-resolution multitransistor array recording of electrical field potentials in cultured brain slices. *J. Neurophysiol.* **96,** 1638–1645 (2006).
6. Eytan, D. & Marom, S. Dynamics and effective topology underlying synchronization in networks of cortical neurons. *J. Neurosci.* **26,** 8465–8476 (2006).
7. Berdondini, L. *et al.* Active pixel sensor array for high spatio-temporal resolution electrophysiological recordings from single cell to large scale neuronal networks. *Lab Chip* **9,** 2644–2651 (2009).
8. Frey, U., Egert, U., Heer, F., Hafizovic, S. & Hierlemann, A. Microelectronic system for high-resolution mapping of extracellular electric fields applied to brain slices. *Biosens. Bioelectron.* **24,** 2191–2198 (2009).
9. Hochberg, L. R. *et al.* Neuronal ensemble control of prosthetic devices by a human with tetraplegia. *Nature* **442,** 164–171 (2006).
10. Blanche, T. J., Spacek, M. A., Hetke, J. F. & Swindale, N. V. Polytrodes: high-density silicon electrode arrays for large-scale multiunit recording. *J. Neurophysiol.* **93,** 2987–3000 (2005).
11. Buzsaki, G., Anastassiou, C. A. & Koch, C. The origin of extracellular fields and currents — EEG, ECoG, LFP and spikes. *Nature Rev. Neurosci.* **13,** 407–420 (2012).
12. Shoham, S., O'Connor, D. H. & Segev, R. How silent is the brain: is there a "dark matter" problem in neuroscience? *J. Comp. Physiol.***192,** 777–784 (2006).
13. Mayford, M., Siegelbaum, S. A. & Kandel, E. R. Synapses and memory storage. *Cold Spring Harb. Perspect. Biol.* **4,** a005751 (2012).
14. Thomas, C. A. Jr, Springer, P. A., Loeb, G. E., Berwald-Netter, Y. & Okun, L. M. A miniature microelectrode array to monitor the bioelectric activity of cultured cells. *Exp. Cell Res.* **74,** 61–66 (1972).
15. Gross, G. W., Williams, A. N. & Lucas, J. H. Recording of spontaneous activity with photoetched microelectrode surfaces from mouse spinal neurons in culture. *J. Neurosci. Methods* **5,** 13–22 (1982).
16. Regehr, W. G., Pine, J., Cohan, C. S., Mischke, M. D. & Tank, D. W. Sealing cultured invertebrate neurons to embedded dish electrodes facilitates long-term stimulation and recording. *J. Neurosci. Methods* **30,** 91–106 (1989).
17. Connolly, P., Clark, P., Curtis, A. S., Dow, J. A. & Wilkinson, C. D. An extracellular microelectrode array for monitoring electrogenic cells in culture. *Biosens. Bioelectron.* **5,** 223–234 (1990).
18. Nam, Y. & Wheeler, B. C. *In vitro* microelectrode array technology and neural recordings. *Crit. Rev. Biomed. Eng.* **39,** 45–61 (2011).
19. Huys, R. *et al.* Single-cell recording and stimulation with a 16k micro-nail electrode array integrated on a 0.18 μm CMOS chip. *Lab Chip* **12,** 1274–1280 (2012).
20. Schwartz, A. B. Cortical neural prosthetics. *Annu. Rev. Neurosci.* **27,** 487–507 (2004).
21. Fee, M. S., Mitra, P. P. & Kleinfeld, D. Automatic sorting of multiple unit neuronal signals in the presence of anisotropic and non-Gaussian variability. *J. Neurosci. Methods* **69,** 175–188 (1996).
22. Brown, E. N., Kass, R. E. & Mitra, P. P. Multiple neural spike train data analysis: state-of-the-art and future challenges. *Nature Neurosci.* **7,** 456–461 (2004).
23. Kauer, J. S., Senseman, D. M. & Cohen, L. B. Odor-elicited activity monitored simultaneously from 124 regions of the salamander olfactory bulb using a voltage-sensitive dye. *Brain Res.* **418,** 255–261 (1987).
24. Siegel, M. S. & Isacoff, E. Y. A genetically encoded optical probe of membrane voltage. *Neuron* **19,** 735–741 (1997).
25. Shoham, D. *et al.* Imaging cortical dynamics at high spatial and temporal resolution with novel blue voltage-sensitive dyes. *Neuron* **24,** 791–802 (1999).
26. Kralj, J. M., Douglass, A. D., Hochbaum, D. R., Maclaurin, D. & Cohen, A. E. Optical recording of action potentials in mammalian neurons using a microbial rhodopsin. *Nature Methods* **9,** 90–95 (2012).
27. Loew, L. M., Cohen, L. B., Salzberg, B. M., Obaid, A. L. & Bezanilla, F. Charge-shift probes of membrane potential. Characterization of aminostyrylpyridinium dyes on the squid giant axon. *Biophys. J.* **47,** 71–77 (1985).
28. Stosiek, C., Garaschuk, O., Holthoff, K. & Konnerth, A. *In vivo* two-photon calcium imaging of neuronal networks. *Proc. Natl Acad. Sci. USA* **100,** 7319–7324 (2003).
29. Higley, M. J. & Sabatini, B. L. Calcium signaling in dendrites and spines: practical and functional considerations. *Neuron* **59,** 902–913 (2008).
30. Rothschild, G., Nelken, I. & Mizrahi, A. Functional organization and population dynamics in the mouse primary auditory cortex. *Nature Neurosci.* **13,** 353–360 (2010).
31. Grinvald, A., Lieke, E., Frostig, R. D., Gilbert, C. D. & Wiesel, T. N. Functional architecture of cortex revealed by optical imaging of intrinsic signals. *Nature* **324,** 361–364 (1986).
32. Nagel, G. *et al.* Channelrhodopsin-1: a light-gated proton channel in green algae. *Science* **296,** 2395–2398 (2002).
33. Bernstein, J. G. & Boyden, E. S. Optogenetic tools for analyzing the neural circuits of behavior. *Trends Cogn. Sci.* **15,** 592–600 (2011).
34. Homma, R. *et al.* Wide-field and two-photon imaging of brain activity with voltage- and calcium-sensitive dyes. *Phil. Trans. R. Soc. Lond. B* **364,** 2453–2467 (2009).
35. Spatz, J. P. & Geiger, B. Molecular engineering of cellular environments: cell adhesion to nano-digital surfaces. *Methods Cell Biol.* **83,** 89–111 (2007).
36. Rutten, W. L. Selective electrical interfaces with the nervous system. *Annu. Rev. Biomed. Eng.* **4,** 407–452 (2002).
37. Fromherz, P. Three levels of neuroelectronic interfacing: silicon chips with ion channels, nerve cells, and brain tissue. *Ann. NY Acad. Sci.* **1093,** 143–160 (2006).
38. Jones, I. L. *et al.* The potential of microelectrode arrays and microelectronics for biomedical research and diagnostics. *Anal. Bioanal. Chem.* **399,** 2313–2329 (2011).

39. Bershadsky, A. D., Balaban, N. Q. & Geiger, B. Adhesion-dependent cell mechanosensitivity. *Annu. Rev. Cell Dev. Biol.* **19,** 677–695 (2003).
40. Wrobel, G. *et al.* Transmission electron microscopy study of the cell-sensor interface. *J. R. Soc. Interface* **5,** 213–222 (2008).
41. Braun, D. & Fromherz, P. Fluorescence interference-contrast microscopy of cell adhesion on oxidized silicon. *Appl. Phys. A* **65,** 341–348 (1997).
42. Iwanaga, Y., Braun, D. & Fromherz, P. No correlation of focal contacts and close adhesion by comparing GFP-vinculin and fluorescence interference of DiI. *Eur. Biophysics J. Biophysics Lett.* **30,** 17–26 (2001).
43. Lambacher, A. & Fromherz, P. Luminescence of dye molecules on oxidized silicon and fluorescence interference contrast microscopy of biomembranes. *J. Opt. Soc. Am. B* **19,** 1435–1453 (2002).
44. Gleixner, R. & Fromherz, P. The extracellular electrical resistivity in cell adhesion. *Biophys. J.* **90,** 2600–2611 (2006).
45. Fromherz, P. in *Neuroelectronic Interfacing: Semiconductor Chips with Ion Channels, Nerve Cells, and Brain* (ed. Waser, P.) Ch. 32, 781–810 (Wiley, 2003).
46. Maccione, A. *et al.* Experimental investigation on spontaneously active hippocampal cultures recorded by means of high-density MEAs: analysis of the spatial resolution effects. *Front. Neuroeng.* **3,** 1–12 (2010).
47. Buitenweg, J. R., Rutten, W. L. & Marani, E. Geometry-based finite-element modeling of the electrical contact between a cultured neuron and a microelectrode. *IEEE Trans. Biomed. Eng.* **50,** 501–509 (2003).
48. Pine, J. Recording action potentials from cultured neurons with extracellular microcircuit electrodes. *J. Neurosci. Methods* **2,** 19–31 (1980).
49. Oka, H., Shimono, K., Ogawa, R., Sugihara, H. & Taketani, M. A new planar multielectrode array for extracellular recording: application to hippocampal acute slice. *J. Neurosci. Methods* **93,** 61–67 (1999).
50. Grumet, A. E., Wyatt, J. L. Jr & Rizzo, J. F. 3rd Multi-electrode stimulation and recording in the isolated retina. *J. Neurosci. Methods* **101,** 31–42 (2000).
51. Kim, J. H., Kang, G., Nam, Y. & Choi, Y. K. Surface-modified microelectrode array with flake nanostructure for neural recording and stimulation. *Nanotechnology* **21,** 85303 (2010).
52. Bruggemann, D. *et al.* Nanostructured gold microelectrodes for extracellular recording from electrogenic cells. *Nanotechnology* **22,** 265104 (2011).
53. Shein, M. *et al.* Engineered neuronal circuits shaped and interfaced with carbon nanotube microelectrode arrays. *Biomed. Microdevices* **11,** 495–501 (2009).
54. Keefer, E. W., Botterman, B. R., Romero, M. I., Rossi, A. F. & Gross, G. W. Carbon nanotube coating improves neuronal recordings. *Nature Nanotech.* **3,** 434–439 (2008).
55. Akaike, N. & Harata, N. Nystatin perforated patch recording and its applications to analyses of intracellular mechanisms. *Jpn. J. Physiol.* **44,** 433–473 (1994).
56. Braeken, D. *et al.* Single-cell stimulation and electroporation using a novel 0.18 µ CMOS chip with subcellular-sized electrodes. *Conf. Proc. IEEE Eng. Med. Biol. Soc.* **2010,** 6473–6476 (2010).
57. Xie, C., Lin, Z., Hanson, L., Cui, Y. & Cui, B. Intracellular recording of action potentials by nanopillar electroporation. *Nature Nanotech.* **7,** 185–190 (2012).
58. Hai, A. & Spira, M. E. On-chip electroporation, membrane repair dynamics and transient in-cell recordings by arrays of gold mushroom-shaped microelectrodes. *Lab Chip* **12,** 2865–2873 (2012).
59. Fendyur, A. & Spira, M. E. Toward on-chip, in-cell recordings from cultured cardiomyocytes by arrays of gold mushroom-shaped microelectrodes. *Front. Neuroeng.* **5,** 21 (2012).
60. Braeken, D. *et al.* Open-cell recording of action potentials using active electrode arrays. *Lab Chip* **12,** 4397–4402 (2012).
61. Spira, M. E. *et al.* Improved neuronal adhesion to the surface of electronic device by engulfment of protruding micro-nails fabricated on the chip surface. *Transducers '07 and Eurosensors XXI* 1247–1250 (IEEE, 2007).
62. Hai, A. *et al.* Spine-shaped gold protrusions improve the adherence and electrical coupling of neurons with the surface of micro-electronic devices. *J. R. Soc. Interface* **6,** 1153–1165 (2009).
63. Hai, A. *et al.* Changing gears from chemical adhesion of cells to flat substrata toward engulfment of micro-protrusions by active mechanisms. *J. Neural Eng.* **6,** 066009 (2009).
64. Hai, A., Shappir, J. & Spira, M. E. Long-term, multisite, parallel, in-cell recording and stimulation by an array of extracellular microelectrodes. *J. Neurophysiol.* **104,** 559–568 (2010).
65. Hai, A., Shappir, J. & Spira, M. E. In-cell recordings by extracellular microelectrodes. *Nature Methods* **7,** 200–202 (2010).
66. Aderem, A. & Underhill, D. M. Mechanisms of phagocytosis in macrophages. *Annu. Rev. Immunol.* **17,** 593–623 (1999).
67. Hayashi, Y. & Majewska, A. K. Dendritic spine geometry: functional implication and regulation. *Neuron* **46,** 529–532 (2005).
68. May, R. C. & Machesky, L. M. Phagocytosis and the actin cytoskeleton. *J. Cell Sci.* **114,** 1061–1077 (2001).
69. Cohen, A., Shappir, J., Yitzchaik, S. & Spira, M. E. Reversible transition of extracellular field potential recordings to intracellular recordings of action potentials generated by neurons grown on transistors. *Biosensors Bioelectronics* **23,** 811–819 (2008).
70. Fendyur, A., Mazurski, N., Shappir, J. & Spira, M. E. Formation of essential ultrastructural interface between cultured hippocampal cells and gold mushroom-shaped MEA — toward "IN-CELL" recordings from vertebrate neurons. *Front. Neuroeng.* **4,** 14 (2011).
71. Robinson, J. T. *et al.* Vertical nanowire electrode arrays as a scalable platform for intracellular interfacing to neuronal circuits. *Nature Nanotech.* **7,** 180–184 (2012).
72. Schoen, I. & Fromherz, P. Extracellular stimulation of mammalian neurons through repetitive activation of Na^+ channels by weak capacitive currents on a silicon chip. *J. Neurophysiol.* **100,** 346–357 (2008).
73. Hofmann, B., Katelhon, E., Schottdorf, M., Offenhausser, A. & Wolfrum, B. Nanocavity electrode array for recording from electrogenic cells. *Lab Chip* **11,** 1054–1058 (2011).
74. Almquist, B. D. & Melosh, N. A. Fusion of biomimetic stealth probes into lipid bilayer cores. *Proc. Natl Acad. Sci. USA* **107,** 5815–5820 (2010).
75. Almquist, B. D. & Melosh, N. A. Molecular structure influences the stability of membrane penetrating biointerfaces. *Nano Lett.* **11,** 2066–2070 (2011).
76. Almquist, B. D., Verma, P., Cai, W. & Melosh, N. A. Nanoscale patterning controls inorganic-membrane interface structure. *Nanoscale* **3,** 391–400 (2011).
77. Tian, B. *et al.* Three-dimensional, flexible nanoscale field-effect transistors as localized bioprobes. *Science* **329,** 830–834 (2010).
78. Duan, X. *et al.* Intracellular recordings of action potentials by an extracellular nanoscale field-effect transistor. *Nature Nanotech.* **7,** 174–179 (2012).
79. Huys, R. *et al.* A novel 16k micro-nail CMOS-chip for *in-vitro* single-cell recording, stimulation and impedance measurements. *Conf. Proc. IEEE Eng. Med. Biol. Soc.* **2010,** 2726–2729 (2010).
80. Doherty, G. J. & McMahon, H. T. Mechanisms of endocytosis. *Annu. Rev. Biochem.* **78,** 857–902 (2009).
81. Cohen-Karni, T., Timko, B. P., Weiss, L. E. & Lieber, C. M. Flexible electrical recording from cells using nanowire transistor arrays. *Proc. Natl Acad. Sci. USA* **106,** 7309–7313 (2009).
82. Sadiku, M. N. O. *Elements of Electromagnetics* (Oxford Univ. Press, 2000).
83. Tian, B. & Lieber, C. M. Design, synthesis, and characterization of novel nanowire structures for photovoltaics and intracellular probes. *Pure Appl. Chem.* **83,** 2153–2169 (2011).
84. Gao, R. *et al.* Outside looking in: nanotube transistor intracellular sensors. *Nano Lett.* **12,** 3329–3333 (2012).
85. Ionescu-Zanetti, C. *et al.* Mammalian electrophysiology on a microfluidic platform. *Proc. Natl Acad. Sci. USA* **102,** 9112–9117 (2005).
86. Lau, A. Y., Hung, P. J., Wu, A. R. & Lee, L. P. Open-access microfluidic patch-clamp array with raised lateral cell trapping sites. *Lab Chip* **6,** 1510–1515 (2006).
87. Martina, M. *et al.* Recordings of cultured neurons and synaptic activity using patch-clamp chips. *J. Neural Eng.* **8,** 034002 (2011).
88. Abidi, A. A. High-frequency noise measurements on FET's with small dimensions. *Electron. Dev., IEEE Trans. on* **33,** 1801–1805 (1986).
89. Voelker, M. & Fromherz, P. Nyquist noise of cell adhesion detected in a neuron-silicon transistor. *Phys. Rev. Lett.* **96,** 228102 (2006).

Acknowledgements

Spira's laboratory is currently supported by EU FP7 MERIDIAN Grant agreement no. 280778., EU FP7 Marie Curie ITG, Grant agreement no. 264872., and the Charles E. Smith and Prof. Elkes Laboratory for Collaborative Research in Psychobiology. A. Hai was supported by a scholarship from The Israel Council for Higher Education.

Additional information

Reprints and permissions information is available online at www.nature.com/reprints. Correspondence should be addressed to M.E.S.

Competing financial interests

The authors declare no competing financial interests.